scientific reports

Check for updates

OPEN

Physiological mechanical forces accelerate the degradation of bovine lung collagen fibers by bacterial collagenase

Yuqing Deng[1], Jacob Herrmann[2,3], Yu Wang[3], Minh Nguyen[3], Joseph K. Hall[3], Jae Hun Kim[3], Michael L. Smith[3], Kenneth R. Lutchen[3], Elizabeth Bartolák-Suki[3] & Béla Suki[3]✉

Collagen fibers, one of the key load-bearing components of the extracellular matrix, contribute significantly to tissue integrity through their mechanical properties of strain-dependent stiffening. This study investigated the effects of bacterial collagenase on the mechanical behavior of individual bovine lung collagen fibers in the presence or absence of mechanical forces, with a focus on potential implications for emphysema, a condition associated with collagen degradation and alveolar wall rupture. Tensile tests were conducted on individual collagen fibers isolated from bovine lung tissue. The rate of degradation was characterized by the change in fiber Young's modulus during 60 min of digestion under various mechanical conditions mimicking the mechanical stresses on the fibers during breathing. Compared to digestion without mechanical forces, a significantly larger drop of fiber modulus was observed in the presence of static or intermittent mechanical forces. Fiber yield stress was also reduced after digestion indicating compromised fiber failure. By incorporating fibril waviness obtained by scanning electron microscopic images, an analytic model allowed estimation of fibril modulus. A computational model that incorporated waviness and the results of tensile tests was also developed to simulate and interpret the data. The simulation results provided insights into the mechanical consequences of bacterial collagenase and mechanical forces on collagen fibers, revealing both fibril softening and rupture during digestion. These findings shed light on the microscale changes in collagen fiber structure and mechanics under enzymatic digestion and breathing-like mechanical stresses with implications for diseases that are impacted by collagen degradation such as emphysema.

Keywords Fiber modulus, Fibril modulus, Waviness, Tensile testing, Computational model

The extracellular matrix (ECM) plays an important role in determining tissue biomechanics. The key load-bearing structural elements of the ECM are the collagen and elastic fibers. Generally, elastic fibers are thought to contribute to Young's modulus in the low-strain regime of the stress-strain curve of tissues, while collagen fibers resist large tensile loads and protect the tissue from mechanical failure[1]. The effective modulus of tissues is an important functional parameter both at the macroscale and the microscale. In the lung, localized microscale variations in modulus are likely optimized to support the physiological functions of the lung[2].

Homeostatic tissue maintenance requires continuous enzymatic digestion and deposition of collagen in the ECM[3]. However, aberrant maintenance such as upregulated excess collagenase can disrupt equilibrium, resulting in collagen damage, a reduction in collagen amount, and the onset of diseases such as emphysema[4]. Following collagenase digestion, lung tissue stiffness decreases and becomes more susceptible to rupture[5]. Furthermore, under continuous mechanical stimulation, such ruptures can lead to further tissue damage due to a redistribution of the stress in the surrounding alveoli and fibers[6]. This is a positive feedback loop that can drive the progression of emphysema.

The tensile mechanics of collagen fibers have been described by a nonlinear recruitment process followed by a linear extension regime of the stress-strain curve[7]. Specifically, for small strains (< 5%), the initially wavy fibrils within a collagen fiber are straightened and recruited to contribute to the total stress, leading to an increase of the slope at higher strains, hence stiffening, along the stress-strain curve. When nearly all fibrils are straightened,

[1]Department of Mechanical Engineering, Boston University, Boston, MA, USA. [2]Department of Biomedical Engineering, University of Iowa, Iowa, IA, USA. [3]Department of Biomedical Engineering, Boston University, 44 Cummington Mall, Boston, MA 02215, USA. ✉email: bsuki@bu.edu

the stress-strain curve becomes linear with a slope that is usually taken to be the modulus of the fiber. The mechanics of the collagen fiber can be described by the waviness distribution of the fibrils, the fibril modulus, and fibril-fibril interactions[1]. How these fibril-level mechanisms, which contribute to the fiber-level mechanics, are influenced by enzymatic digestion is not fully understood. Additionally, how mechanical stresses acting on collagen fibers influence the ability of enzymes to digest the fibers is controversial[8]. Indeed, it is unclear whether the application of force on a fiber accelerates or hinders degradation, and the results may depend on the specifics of the experimental conditions such as (1) the tissue origin of the collagen fibers, (2) the enzyme type employed, and (3) the magnitude and dynamics of loading.

We previously reported that the degradation of lung tissue strips by bacterial collagenase was accelerated by both dynamic and static forces[5]. In the current study, we aimed to investigate how mechanical forces in the lung influence the rate of degradation of collagen fibers and fibrils. Specifically, we hypothesized that lung collagen fibers exhibit an accelerated rate of degradation when experiencing large forces due to high pre-stress and during deep inspirations. To test this hypothesis, we isolated collagen fibers from bovine lungs, which are comparable in size to human lungs. The quasi-static fiber stress-strain curves were obtained before and after digestion in the presence or absence of a static force or intermittent large stretches. The magnitudes of the tensile force were chosen to produce stresses that corresponded to those predicted on collagen fibers in the lung[9]. Alterations in fiber microstructure were examined using a scanning electron microscope (SEM) and the results were interpreted by an analytical and a computational model of the fiber.

Results

Lung collagen fiber isolation

Individual collagen fibers were manually isolated from decellularized and elastase-degraded bovine lung tissue. Concentrations of released total proteins into the supernatant during the isolation steps from four independent isolations are summarized in the Supplementary Fig. S1. Figure 1 demonstrates different stages of the isolation process using fluorescent microscopy and SEM imaging. Note that collagen fibers lose their native waviness only after elastin is enzymatically degraded (Fig. 1b), indicating that elastin maintains residual stress in the tissue even after decellularization and without any external loading. Fiber diameters were measured with variation between 0.8 and 3.8 µm before elastase digestion showing a slight decrease to a variation between 0.6 and 3.3 µm after elastase digestion. However, no further fiber diameter changes were observed after proteoglycan digestion by trypsin. Examination of manually isolated fibers (Fig. 1c, d) with SEM confirms fiber composition of collagen fibrils with diameters approximately 50–100 nm and characteristic 67 nm D-banding[7]. The larger diameters likely resulted from several smaller fibers coalescing into a single fiber during isolation (Fig. 1e).

Effects of proteoglycans on collagen fiber properties

To examine whether there were interactions between proteoglycans and collagen that could affect fiber mechanics[10], we carried out fiber tensile tests before and after 60 min of trypsin digestion. The stress-strain curves from 5 fibers were not altered by trypsin treatment (Supplementary Fig. S2). The mean ± SD of the percent change in modulus was 0.1 ± 0.1%, indicating that proteoglycans had little effect on fiber mechanical properties.

Tensile testing

Panel (a) in Fig. 2 shows a single fiber in the measurement system and panel (b) depicts a representative stress-strain curve before digestion, demonstrating a non-linear region below 5% strain followed by a linear region. The stress-strain curves of all fibers without digestion are plotted in Fig. 3a. Fiber modulus was computed as the slope of a linear regression to the data between 7 and 10% strains. The mean ± SD of the modulus was 61.9 ± 39.4 MPa, with a skewed distribution. A log-normal distribution fits the data well with an R^2 value of 0.88 (Fig. 3b).

Figure 4a displays the stress-strain curves of a representative fiber during digestion in the intermittently stretched (up to 10% strain every 10 min for 1 h) group (D-i). Over the course of digestion, the linear region of the curve gradually shifted to higher strains and the modulus decreased from 97.8 ± 39.8 to 26.2 ± 23.0 MPa

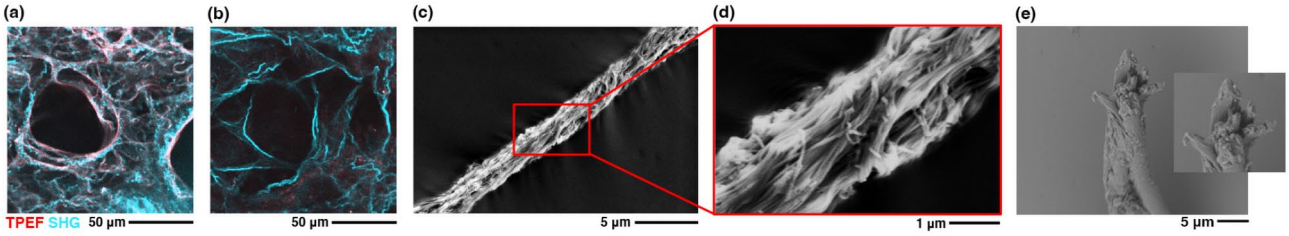

Fig. 1. Lung collagen fiber isolation. Decellularized bovine lung samples (**a**) exhibit pairs of wavy and taut fibers via second harmonic generation (SHG, cyan) and two-photon excited fluorescence (TPEF, red), respectively, associated with collagen and elastin in the unstretched tissue strip. Elastase treatment obliterates the fiber structures from the TPEF signal, leaving behind loosely associated fibers with strong SHG signal and reduced waviness (**b**). Fibers isolated from the decellularized and elastase-degraded tissues exhibit parallel bundles of smaller fibrils under scanning electron microscopy (**c**) with banding patterns characteristic of collagen observable at high magnification (**d**). (**e**) SEM image of the tip of an aggregated collagen fiber. Inset: zoomed image of the fiber tip.

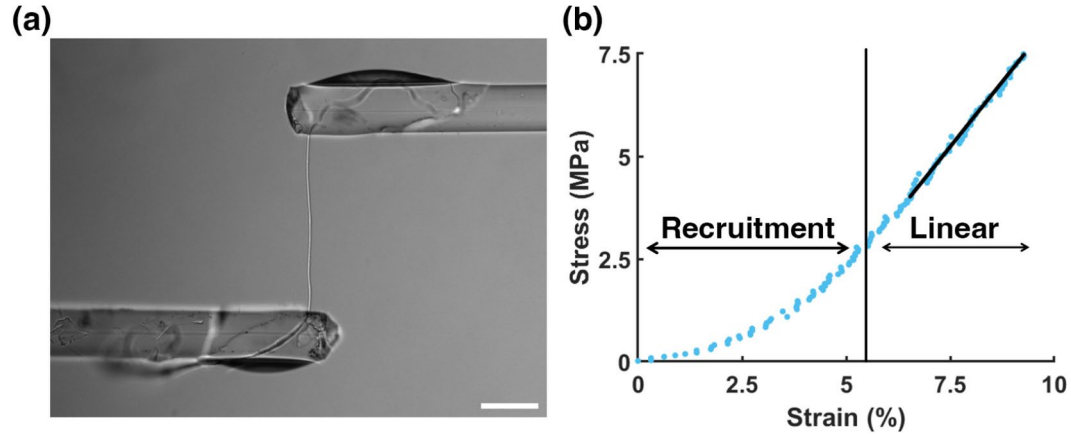

Fig. 2. (**a**) An isolated collagen fiber was attached by epoxy glue to the tips of two optical fibers on the collagen fiber stretcher system. Scale bar: 100 μm. (**b**) Example stress-strain curves exhibiting a recruitment and a linear regime. The black line depicts the slope of the curve in the linear regime.

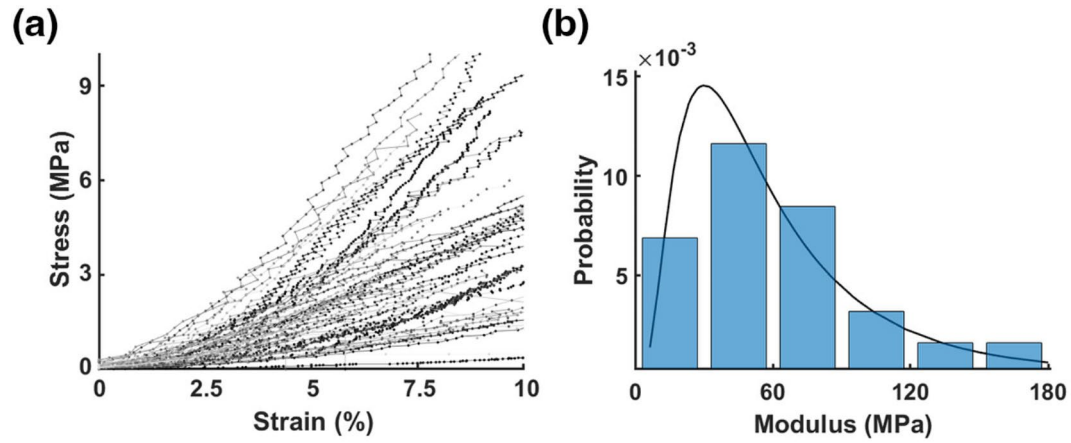

Fig. 3. (**a**) Stress-strain curves of all fibers without enzymatic digestion ($n=63$). (**b** Probability distribution of fiber modulus and the fit of a log-normal distribution with an arithmetic mean and SD of 63.1 and 50.2, respectively ($R^2=0.88$).

(Fig. 4b). To exclude the possibility that the decrease in modulus was caused by pure mechanical stretching, the control group (C) received the same stretch treatment (without collagenase) as the D-i group. Any change in modulus was characterized by the ratio of modulus after digestion to its initial value. Figure 4c summarizes the digestion results whereas Fig. 4d shows the experiment protocol. The modulus in the C group remained constant during the 60 min period, indicating that intermittent tensile tests did not alter fiber modulus (Fig. 4c). A comparison between fibers in the C and combined digested groups including pure digestion (D), digestion in the presence of static stress (D-3: 300 kPa or D-6: 600 kPa), and D-i revealed a significant decrease in modulus ($P<0.05$). Furthermore, the decrease in modulus observed in the D-i group was significantly larger than in the D group fibers ($P<0.001$). An increased degradation rate was also observed in the presence of both static stresses (D-3 and D-6) group ($P<0.01$). While the D-6 group ($n=11$) showed a trend towards increased digestion rate compared to the D-3 group ($n=11$), the differences were not statistically significant. However, the stiffness of 2 fibers in the D-3 group dropped to unrealistically low values below 10% of the mean after digestion. When these 2 fibers were omitted from the analysis, the difference between the D-3 and D-6 groups reached statistical significance ($P<0.05$). Interestingly, an F-test also revealed a significantly lower variance in the D-6 group compared to the D-3 group ($P<0.01$), suggesting a more consistent response to digestion under higher stress conditions. Additionally, 3 fibers broke during digestion in the D-6 group whereas only 1 fiber broke in the D-3 group. In selected fibers ($n=8$), SHG imaging showed clear evidence of digestion-induced decrease in SHG signal to $85\pm10\%$ ($P=0.02$) of its initial intensity, implying that there was less collagen in the fiber at the end the digestion (see Supplementary Fig. S5). This is consistent with the total protein analysis showing more released proteins after collagenase than trypsin (see Supplementary Fig. S1).

The effects of digestion on fiber failure mechanics were assessed by comparing the results obtained in all three digestion groups with those obtained in fibers without digestion. Since stretching without enzyme did not

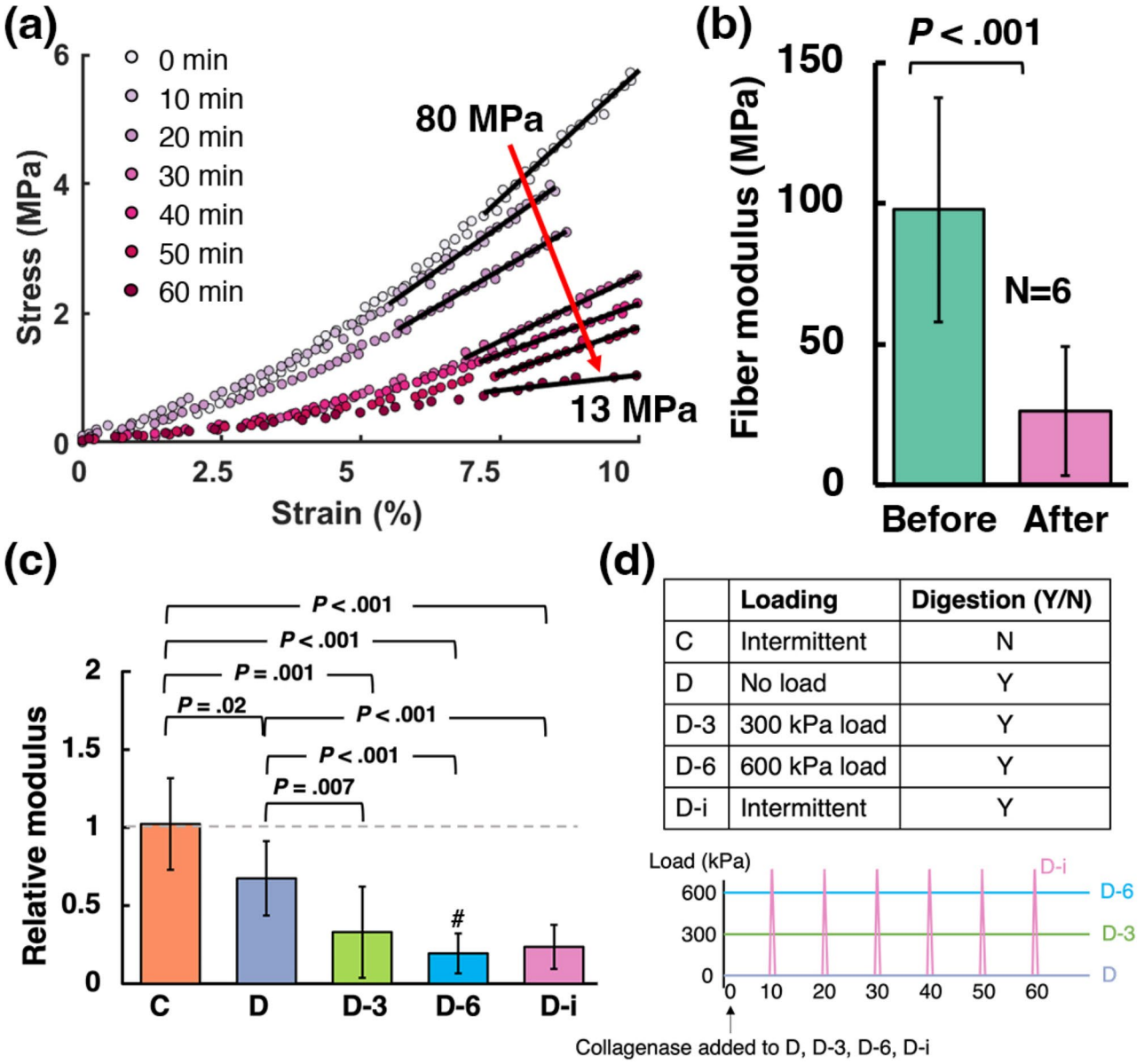

	Loading	Digestion (Y/N)
C	Intermittent	N
D	No load	Y
D-3	300 kPa load	Y
D-6	600 kPa load	Y
D-i	Intermittent	Y

Fig. 4. (**a**) Stress-strain curves of a representative fiber obtained during digestion. Data were collected at 10-min intervals. Black lines: linear fits over the highest 3% strain region. The slopes of the top and bottom lines are shown. (**b**) Mean ± SD of measured fiber modulus before and after 60 min of digestion in the D-i group. (**c**) Normalized moduli in all groups with significance levels above the graph showing differences between groups. C: control; D: digested group; D-3: digested with a static force of 300 kPa; D-6: digested with a larger static force of 600 kPa; D-i: digested with intermittent force. #: $P < 0.05$ between D-3 and D-6 when 2 outliers in D-3 were excluded (see text). (**d**) Table showing the groups and the corresponding treatment protocols. Further details of these groups are summarized in Table 1.

influence fiber mechanics, non-digested fibers failed at initial stretch and at 60 min were both included in the analysis. Yield stress was obtained by finding the yield point on the stress-strain curves (Fig. 5a, inset). The yield stress exhibited a significant decrease from 5.9 ± 1.4 to 2.4 ± 0.5 MPa ($P < 0.05$) when collagenase was applied. The strain that was required to generate the maximum force was significantly lower before than after digestion (Fig. 5b). Interestingly, the maximum stress was not different between digested and control fibers.

SEM images

Representative fibril images before and after collagenase digestion are shown in Fig. 6. Occasional crimps on collagen fibrils can also be observed (see arrow) that are similar to those found on fibrils in tendon[11]. D-banding of collagen fibrils was clearly observed in control fibers but not in digested fibers (Fig. 6a). Fibril diameter significantly increased from 59.5 ± 14.5 nm in the C group to 71.6 ± 14.3 nm in digested fibers ($P < 10^{-16}$). The beta distribution (Eq. 10) was fitted to the measured distribution of waviness in both the control and the digested

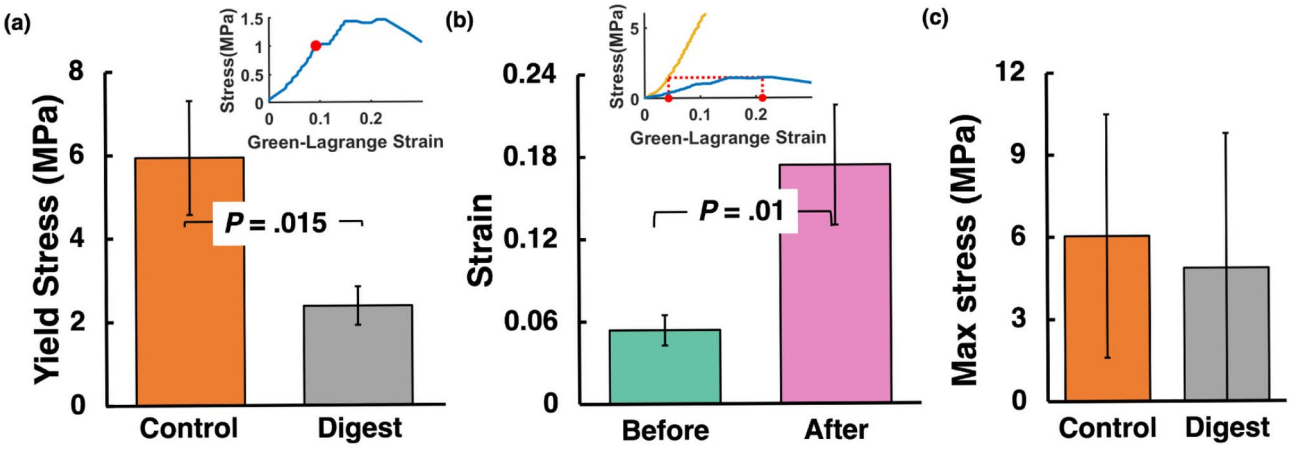

Fig. 5. (**a**) Yield stress obtained from the stress-strain curves of fibers with ($n=21$) and without ($n=18$) digestion. The group Digest includes fibers from digested groups (D, D-i, and D-3), combined for the analysis. Inset: an example curve with a red dot indicating the yield point. (**b**) The strain corresponding to the maximum stress in fibers after digestion and the strain at which undigested fibers reached the same stress ($n=12$). Inset: example curves with two red dots corresponding to the strain values that were used for the analysis. The blue curve is the same data as in the inset in panel (**a**) while the yellow curve is the data before digestion. Error bars represent standard errors.

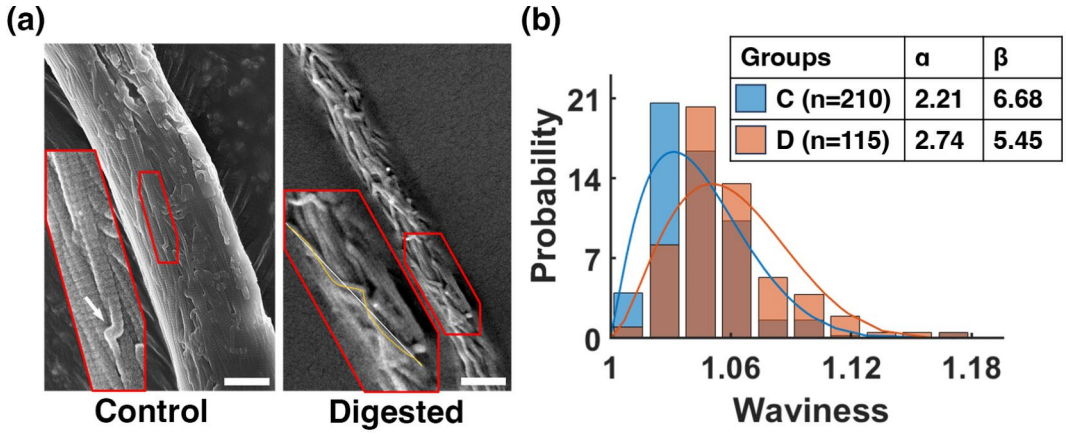

Fig. 6. (**a**) SEM images of collagen fibers without (left) and after enzymatic digestion (right). Scale bar: 1 μm. Red boxes are zooms into the fiber showing D-bands (Control) and the white arrow indicates a crimp on the collagen fibrils and an enlarged digested fiber image with the contour line (l, yellow) and end-to-end line (l_{ee}, white) for one fibril (Digested). (**b**) Probability distribution of fibril waviness measured from SEM images of fibers in the C group and D group. Curves: Fits of the beta probability distribution to the data. Fitting results are listed in the table. The α and β values are the parameters of the beta distribution in Eq. 10.

fibers, which showed that the peak of the distribution shifted to a higher value for the digested fibers, indicating a preferential digestion of fibrils with low waviness (Fig. 6b).

The fibrils were mainly oriented along the long axis of the fiber. Comparing the spatial frequency distributions generated by the 2D Fast Fourier Transform analysis, a significantly lower ($P<0.05$) aspect ratio of fibril orientation in the digested (3.1 ± 0.9) versus control (4 ± 2.2) fibers indicated a change in fiber microstructure (Supplementary Fig. S3).

Analytical and computational modeling

Fitting the analytical model of the fiber (Eq. 13) to measured stress-strain curves allowed us to evaluate the changes in fibril modulus during digestion. Next, the fiber modulus was calculated from the model (Eq. 14) and compared with direct experimental measurements (Fig. 7a). The results showed a high degree of linearity, with an R^2 value of 0.98, between model predictions and experimental data. Including all fibers before digestion, the estimated average modulus of the intact fibers was 57 MPa whereas that of the fibrils was 66 MPa. Additionally, the predicted fibril modulus decreased to 46% of its initial value in the D-i group (Fig. 7b). Within the same digestion group, the modulus at the fiber level decreased to only 23.7% of its initial value.

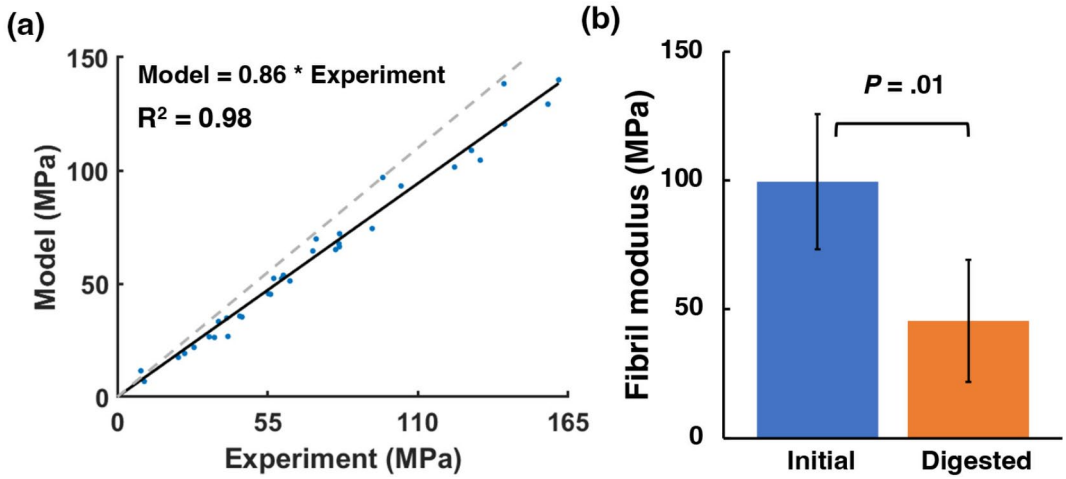

Fig. 7. (**a**) Regression between experimentally measured initial fiber modulus and model predictions ($n = 34$). Blue dots: individual modulus results. Gray dash line: line of identity. Black line: linear fitting of the result with fixed intercept at the origin. Modulus values were experimentally measured by straight line fitting of the data in the linear region of the stress-train curve (between 7 and 10% strains). Model prediction of fiber modulus was obtained by using the estimated fibril modulus in Eq. (14) to predict fiber modulus. (**b**) Fibril modulus predicted from the analytical model for fibers in the D-i group. Error bars represent standard errors.

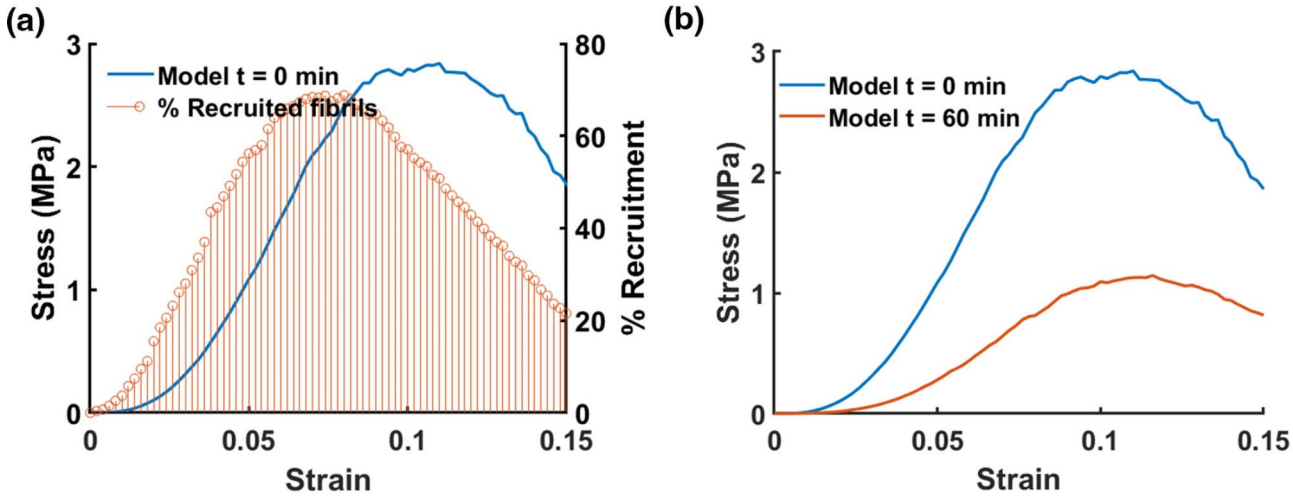

Fig. 8. (**a**) A simulated stress-strain curve with the corresponding percent of recruited fibrils superimposed. (**b**) Stress-strain curves from the computational model of a fiber in D-i group before and after digestion.

Experimental results, including the reduced fibril modulus (Fig. 7b) and a low-waviness preferential digestion (Fig. 6d), were incorporated into the computational model to simulate the progressive changes in the stress-strain curve during digestion. The computational model was able to capture the recruitment process during stretching of a fiber (Fig. 8a) and reproduce how the experimental stress-strain curves changed during digestion (Fig. 8b vs. Figure 4a and Supplementary Table 1). The computational model was then used to compute the failure regions in a fiber before and after digestion. From 10 repeated simulations mimicking the protocol in the D-i group, the results showed that the fiber failure stress decreased by $17.6 \pm 1\%$ after digestion, indicating that fiber weakening by enzymatic digestion was enhanced by mechanical forces. Additionally, approximately 40% of fibrils failed both in the D-3 and D-i groups during digestion. Interestingly, in the D-i group, 96% of the fibrils failed during the intermittent stretching, suggesting that intermittent mechanical perturbations can cause substantial damage by rupturing fibrils in the presence of digestive enzymes.

Discussion

In this study, the mechanical properties of individual lung collagen fibers were obtained by quasi-static tensile testing during enzymatic digestion using bacterial collagenase. All fiber stress-strain curves exhibited both a recruitment phase with increasing modulus at low strains and a linear regime before plastic deformation.

Mechanical forces, including both static and intermittent, significantly accelerated the degradation process indicated by a larger drop in fiber modulus following 60 min of enzyme treatment. Digestion also lowered the yield stress and produced a higher strain at maximum stress in fibers after digestion than the strain at which undigested fibers reached the same stress. Based on measured fibril waviness, an analytical model was developed to estimate the average fibril modulus from fiber stress-strain curves. The results showed that on average, fibril strain was lower than fiber strain and the estimated fibril modulus was 16% higher than fiber modulus before digestion. Computational modeling also suggested that 40% of the fibrils ruptured during digestion under mechanical stresses.

A discrete computational model of parallel fibrils that incorporated force-dependent digestion and rupture probabilities could account for all aspects of the data (Supplementary Table 1). The sensitivity of fiber modulus reduction, defined as the ratio of final to initial moduli, to fibril rupture and digestion was examined by varying C and $F_{f,10}$ in Eqs. (15) and (16), respectively (Supplementary Table 2). Similar reductions in fiber modulus could be achieved by increasing digestion or rupture probabilities. Notably, fibers in the D-i and D-3 groups, digested in the presence of intermittent and static strain respectively, showed similar reductions in modulus. However, these groups likely follow different mechanisms. Compared with the D group (pure digestion), with more intermediate stretches during D-i, the stronger reduction in fiber modulus was dominated by increased fibril ruptures. On the other hand, with a higher value of F_f in the fibril digestion probability (Eq. 16), D-3 fibers had more digestion-weakened fibrils, leading to a softer fiber.

Mechanical behavior similar to our stress-strain curves in the C group was found in collagen fibrils isolated from tendons in which the observed molecular straightening, stretching, and gliding correlated with the heel and linear regions of the curve[7]. This is consistent with the analytical model of the nonlinear fiber stress-strain relationship originating from the recruitment of wavy fibrils (Eq. 13). Our fiber modulus values ranged from 10 to 160 MPa with a skewed lognormal distribution (Fig. 3b). The same type of distribution was found to describe lung tissue strip stiffness which is determined by both elastin and collagen fibers[5]. The wide variation in modulus at the fiber level can be due to differences in (1) the relative amounts of types I and III collagen, (2) crosslinks content, and (3) developmental status[12–16]. A combination of experiments and modeling suggested that this mechanical heterogeneity at the level of collagen fibers may play an important role in the transfer of mechanical cues from the ECM to cells which may contribute to homeostatic tissue maintenance[17].

The analytic model (Eq. 12) allowed us to estimate the average fibril modulus within a fiber. The model is based on the measurement of the waviness distribution. The mean and SD of modulus in group C were 99.4 ± 58.6 MPa. This value is lower than the 1 to 5 GPa range reported in the literature[12]. However, most of these values correspond to tendon fibrils, in which the amount and type of crosslinking such as bivalent vs. trivalent bonds significantly contribute to fibril mechanics[12]. Compared to tendon for which less than 5% of total collagen is type III, 33% of total collagen in the lung is type III[18,19]. It was reported that tissue modulus inversely correlates with the amount of type III collagen, decreasing from 150 to 10 MPa as type III content increased[16]. Additionally, most of the GPa-range modulus values were obtained in dry collagen fibrils in which a high molecular packing density results in an increased density of noncovalent interactions, thus requiring a larger force to achieve sliding of molecules on each other during tensile loading. The bending modulus of dry fibrils was reported to be in the range of 1 to 4 GPa whereas that of hydrated fibrils was between 70 and 170 MPa[20]. The only fibril modulus from lung tissue we are aware of reported values that were lower than ours ranging from about 0.7 MPa to 20 MPa[21]. These values were obtained through nanoindentation on the fibril surface. Due to the mechanical anisotropy of collagen fibers, comparison between nanoindentation and uniaxial tensile tests, which probe mechanics in different modes of deformation, can produce different moduli[12,22]. Thus, while our estimated fibril modulus values are lower than several values reported in the literature on tendon fibrils, they are higher than values from lung collagen fibrils. The differences are likely due to hydration state, modes of deformation, crosslink types and their density as well as collagen types.

The results that mechanical forces accelerate enzymatic digestion of lung collagen fibers are consistent with previous findings in lung tissue[5]. It is important to note that the role of mechanical forces on collagen degradation depends on[8,23–25]: (1) collagen types in the sample, (2) enzyme types and their concentration, (3) temperature, hydration and pH, (4) magnitude of force or strain as well as (5) strain rate. Several studies have found that strain stabilized collagen and protected it from degradation[26–29] whereas others reported that strain increased the degradation rate[5,30,31]. Yeganegi et al. reported that in decellularized porcine pericardium under biaxial stretch, cathepsin K-induced degradation rate increased with strain, whereas MMP-1-, MMP-8-, and MMP-9-mediated degradation showed a V-shaped dependence on strain, exhibiting first a decrease, reaching a minimum followed by an increase[32]. Additionally, a V-shaped curve was also reported when collagen fibers were digested with bacterial collagenase[33]. This behavior is similar to our previous finding in lung tissue where 20% uniaxial stretch was digestion-protective compared to 0 or 40% and 80% strains[5]. Thus, at sufficiently large but still physiologically relevant strains degradation by any of the reported enzymes appear to be enhanced by strain. Additionally, increasing strain rate further amplifies this dependence[5].

We also note that the application of bacterial collagenase, which has a stronger activity than tissue collagenases such as MMP-1, may also contribute to the results[27]. As bacterial collagenases have been widely used in in vitro studies related to the mechanisms of collagen digestion, using this enzyme can still provide insight into the role of collagenase in disease caused by collagen damage and failure[5,33,34]. Additionally, collagenase from Clostridium histolyticum was found to induce lung hemorrhage when applied on dog lung surface or when injected into the thorax of mice[35]. A gene coding for bacterial collagenase has also been identified in the lungs of Leptospira-infected hamsters, which is thought to be involved in pulmonary hemorrhage[36].

Regarding the mechanism of how mechanical forces accelerate collagen digestion, we note that overall enzyme activity can be described as a biased random walk of the enzyme along the fiber interrupted by binding and cleaving events[37,38]. The digestion rate depends on the probability, p_{on}, that an enzyme binds to a molecule

on the fiber and the probability, p_{off}, that the enzyme hops off the binding site which is usually accompanied by cleaving the molecule. Within a given time interval, higher values of p_{on} and/or p_{off} allow more frequent binding and cleaving events which result in a faster degradation. In a single molecule study, while applied forces markedly increased type I collagen cleavage rate by MMP-1, bacterial collagenase did not show an appreciable force-dependent digestion rate[31]. However, collagenase binding sites on the molecule are hidden in the overlap region of fibrils by C-telopeptides[39]. This is a mechanism that protects the fibril against digestion, and it was suggested that collagenases can only proteolyze the fibril after the C-telopeptides are removed. An atomistic model simulation also revealed that thermal fluctuations can temporarily rearrange the triple helices within overlap regions allowing binding sites to become accessible[40]. Since mechanical forces on the fibrils can extend the D periods, it is reasonable to assume that stretch also unfolds these hidden binding sites. This in turn increases p_{on} in a force-dependent manner that can account for our observed results. Although these predictions warrant further experiments, they are also supported by our SEM results because the probability of finding fibrils with low waviness was reduced by digestion (Fig. 6b), indicating a preferential digestion in extended fibrils, i.e. low-waviness fibrils.

Fiber failure depends on the fibril waviness distribution[41]. While the formation of fibril crimps was not studied here, we observed a right shift of the waviness distribution following digestion (Fig. 6b). This shift in the waviness distribution was also reflected in the stress-strain curves because the nonlinear region extended to higher strains (Fig. 4a). However, from the computational simulation, a preferential digestion alone cannot explain the large shift in waviness seen in SEM images. One possibility is that some digested fibrils that were dangling on the fiber surface were counted in the waviness distribution, but these fibrils did not generate force. These fibrils could have moved freely around the fiber and presented higher waviness compared to the case when they were packed within the fiber (Supplementary Fig. S4). Furthermore, a significant difference in waviness was found between measurements from AFM and SEM, indicating the effects of water on fibrils organization (Supplementary Fig. S4). Nevertheless, the increase in fibril diameter in the hydrated condition and fibril reorganization found from SEM images (Fig. 6) indicated a potential molecular reorganization within the fibrils following digestion[42]. After digestion, there were fewer fibrils contributing to the total force due to rupture, thus more fibrils needed to be recruited to generate the same amount of force, leading to a higher fiber extension and reduced fiber yield stress (Fig. 5).

It is important to point out that after decellularization and elastase treatment, some extracellular matrix components such as laminin, fibronectin and glycosaminoglycans could have still remained in the collagen network before fiber isolation[43,44]. Although these components probably have little effects on collagen fiber mechanics, they can occupy part of the cross-sectional area of collagen fibers[45]. In the analytical model, the entire cross-sectional area of a collagen fiber was assumed to be due to fibrils. Thus, the model likely underestimated fibril modulus because of the packing efficiency of fibrils into a circular fiber. The ratio of measured and predicted fiber modulus did not show any relationship with the experimental fiber modulus and was approximately constant with mean $\pm$ SD of 1.2 ± 0.1. Another limitation of the computational model is that whether the enzyme digests fibrils only from the surface or homogeneously throughout the entire fiber volume wasn't considered. In our computational model, all fibrils had the same digestion and rupture probabilities between each stretch. The results demonstrated that only 2–6% of fibrils ruptured between 0 and 60 min in the D group. Interestingly, the shape of our stress-strain curves following digestion was more similar to the computational simulations of volumetric digestion than surface digestion[46] potentially indicating that bacterial collagenase may digest volumetrically. Indeed, one type of bacterial collagenase was shown to diffuse into a fiber effectively producing a volumetric digestion of collagen microfibrils[47]. To conclude, by implementing experimental observations into the computational model, the predicted stress-strain curves successfully matched experimental curves (Fig. 8). However, since our model did not consider inter-fibrillar interactions, the failure regime of the predicted curves did not match those of the experimental stress-strain curves.

In summary, to our knowledge this is the first report on individual lung collagen fiber and fibril mechanics before and after enzymatic digestion. Our data suggest that alveolar walls in the lung that are under higher-than-average mechanical forces have a higher risk of degradation, thus lowering the yield and rupture stresses. These results may have implications for diseases such as pulmonary emphysema in which remodeling or direct damage of the lung tissue occurs via enzymatic degradation.

Methods

Lung collagen fiber isolation

Fresh bovine lung samples (Research 87, Boylston, MA, USA) underwent decellularization through a series of sequential 24-hour washes[43] (four independent isolation). Briefly, lung parenchymal strips (~ 10 mm × 3 mm × 3 mm) were weighed and shaken at 4 °C for 24 h (Fraction 1) in 2% Triton-X-100 buffer (10 ml/gram tissue). The solution was replaced by fresh buffer after 4 and 8 h. The tissue was then placed into a 0.1 M sodium chloride (NaCl) solution with 0.1% sodium dodecyl sulfate (SDS) and shaken at 4 °C for 24 h to remove the remaining cellular structures (Fraction 2). The SDS/NaCl buffer was replaced by deionized water and the tissue was shaken at 4 °C for another 24 h (Fraction 3). Subsequently, the decellularized tissue was subjected to enzymatic treatment using porcine pancreatic elastase (Elastin Products, Owensville, MO, USA) at a concentration of 60–80 units g^{-1} in PBS at 37 °C for 2 h to remove elastin fibers (Fraction 4). Following decellularization and elastin digestion, the resulting samples were nearly pure collagen networks, which were subsequently washed with PBS and stored at −20 °C before use. The BCA Assay Kit was used to measure the protein concentrations in each fraction from 4 independent isolation according to the manufacturer's instructions (Catalog No. PI23227, Thermo Scientific-Pierce).

Before isolating individual collagen fibers, frozen collagen networks were thawed and subjected to a PBS wash on a rotator at room temperature for 10 min. Individual fibers were mechanically teased apart using round-

tipped glass rods and isolated from the collagen network using #5S forceps (Electron Microscopy Science). Isolated fibers were then transferred onto a charged glass slide and stored at 4 °C. All subsequent experimental procedures were conducted within 2 weeks.

Fiber tensile testing

The tensile testing apparatus described by Bradshaw et al.[48] was prepared by first aligning the tips of two optical fibers of 80-µm diameter (Thorlabs, Newton, NJ, USA). The elastic modulus (E) of the optical fibers was assumed to be 70 GPa, allowing calculation of the bending stiffness (K) of each optical fiber according to its measured diameter D_0 and length (L_0), treating the optical fiber as a cantilevered cylindrical thin beam:

$$K = \pi \frac{3{D_0}^4}{64L_0^3}E \tag{1}$$

A small bead of epoxy adhesive was placed onto the tip of each optical fiber. A single dried isolated collagen fiber was mounted via forceps across the two beads of epoxy adhesive, which was allowed to cure overnight at room temperature (see Fig. 2a). The mounted collagen fiber assembly was then lowered into 50mM TES buffer (Sigma-Aldrich, Saint Louis, MO, USA) between two glass coverslips, and the tensile testing apparatus was prepared for stretching and microscopic imaging. One optical fiber was attached to a stationary support, while the other optical fiber was attached to a moving support driven by a motorized linear actuator with a constant displacement rate of 3 µm s^{-1} for about 40 s Force on the collagen fiber (F) was calculated from the image-based vertical bending displacement of the distal tip of the stationary optical fiber (Δy_s) and its bending stiffness K_s obtained from Eq. (1):

$$F = K_s \Delta\, y_s \tag{2}$$

The vertical bending displacement of the moving optical fiber (Δy_m) was then calculated:

$$\Delta\, y_m = \frac{F}{K_m} \tag{3}$$

where K_m is the bending stiffness of the moving optical fiber. The vertical distance between the two optical fibers (d) was computed according to the initial span (d_0) and the change imposed by the difference between the total actuator displacement (Δy_a) and sum of optical fiber bending displacements:

$$d = d_0 + \Delta\, y_a - (\Delta\, y_s + \Delta\, y_m) \tag{4}$$

The collagen fiber stretch ratio (λ) was then computed relative to the initial arc length of the collagen fiber (L):

$$\lambda = \begin{cases} \frac{d}{L} & d > L \\ 1 & \text{otherwise} \end{cases} \tag{5}$$

Note that this formulation only accounts for stretch once the collagen fiber is taut between the two optical fibers. The initial collagen fiber diameter (D) estimated by microscopy was used to compute engineering stress, assuming a circular fiber cross-section:

$$\sigma = F \cdot \left(\frac{1}{4}\pi\, D^2\right)^{-1} \tag{6}$$

Engineering uniaxial strain was then calculated as:

$$\varepsilon = \lambda - 1 \tag{7}$$

Green-Lagrange strain was calculated as:

$$\varepsilon_{GL} = \frac{1}{2}\left(\lambda^2 - 1\right) \tag{8}$$

Enzymatic digestion of fibers

For the proteoglycan digestion experiment, Trypsin Solution (10×9002-07-7 - Sigma-Aldrich) was used at a final concentration of 0.25%. Trypsin Solution 10× is a 2.5% solution of 1:250 trypsin (1:250 designation indicates the tryptic activity based on standardized testing according to the manufacturer) and the suggested final concentration is 0.05–0.25% for one –two hours. A baseline stress-strain curve was collected without stretching the fiber to strains that would cause yield. Next, trypsin was added to the PBS solution to digest proteoglycans for 60 min followed by another measurement of the stress-strain curve.

During collagenase digestion, bacterial collagenase (Sigma-Aldrich, collagenase from clostridium histolyticum, Catalogue C0130) and calcium chloride ($CaCl_2$) (Sigma-Aldrich, Saint Louis, MO, USA) were added to the buffer solution following an initial tensile test. The concentrations of the enzyme and $CaCl_2$ were adjusted to achieve final values of 0.5 mg/ml and 0.36 mM, respectively. The following four groups of fibers were tested over a period of 60 min: (1) a control (C) group, in which fibers were stretched to a strain of 10% every 10 min without enzymatic treatment; (2) a digestion (D) group, in which fibers were digested in the absence

of mechanical forces, mimicking fiber digestion without stress in collapsed regions of the lung; (3) a group of fibers that were digested in the presence of small (D-3) or large static stress (D-6) that were chosen to mimic the stress on collagen fibers at end-expiration and end-inspiration; and (4) a group in which fibers were digested and intermittently stretched to a strain of 10% every 10 min (D-i). Note that the C group was given the same loading conditions as the D-i group but without bacterial collagenase. The 10% strain was based on the estimated strain on collagen fibers in the normal lung at total lung capacity (TLC). The applied force and strain in groups D-3, D-6, and D-i were chosen based on an estimated fiber prestress and strain at TLC[9]. The experimental groups are summarized in Table 1.

Digested fibers were also imaged using SEM or AFM (see below). Fibers were first placed on top of a charged glass slide and exposed to bacterial collagenase at 37℃ without applied force for 60 min as described above. The enzyme was removed by washing the slide 3 times with di-H_2O. The fibers were then dried in a hood overnight before imagining.

SHG microscopy was used on selected fibers to quantify the collagen content before and after digestion (Supplementary Fig. S5). Collagen fibers were glued on a glass slide. The SHG signal intensity of the fibers was calculated as the sum of the signal across the projection image of a fiber, which correlates directly with the amount of organized type I collagen. By comparing the SHG signal intensities before and after the digestion process under the same environment and acquisition setting, changes in collagen content and structure were tracked.

SEM imaging

The dried samples were coated with Au/Pd using a sputter coater system (Cressington Scientific Instruments, Watford, UK) for 10 s. SEM imaging was conducted using a Zeiss Supra 55VP instrument (Carl Zeiss, Jena, Germany), operated at 3–5 kV depending on the magnification.

Contour length l and end-to-end distance l_{ee} of individual fibrils on fibers were measured by manually tracing the fibrils on the images. The waviness w_f of collagen fibrils was defined as:

$$w_f = l/l_{ee} \tag{9}$$

The fibril waviness data were fitted with a beta probability distribution function defined as:

$$p(w_f) = \frac{(w_f - 1)^{\alpha - 1}(w_{max} - w_f)^{\beta - 1}}{B(\alpha, \beta)(w_{max} - 1)^{\alpha + \beta - 1}}, \tag{10}$$

where $w_{max} = 1.18$ is the maximum waviness and $B(\alpha, \beta)$ is the beta function of the variables α and β.

To quantify fibril orientation, a 2D Fourier analysis was performed using the Fast Fourier Transform function of Matlab (Mathworks, Natick, MA, USA)[49]. For both the horizontal and vertical directions, spatial frequencies between the 58th and 59th percentiles were selected and plotted in the 2D frequency space. The resulting data distribution was then fit with an ellipse, and the aspect ratio of the major and minor axes was computed for each image and compared between groups (Supplementary Fig. S3).

Analytical modeling

To characterize the mechanical properties of the fibers, an analytical model was developed closely following the derivation of our previous stress-strain model of wavy fibers in the alveolar wall[9]. Briefly, fibers are conceptualized as a set of non-interacting linearly elastic springs arranged in parallel each representing an individual fibril. If we assume that the fiber is straight and has a unit length, fibril waviness w_f found from the SEM images can be used to represent the distribution of fibril resting lengths given by Eq. (10). Assuming the fibrils undergo the same extension as the fiber with no slippage during stretching, the stress generated by a fibril with waviness w_f is given by

$$\sigma_f = \begin{cases} 0 & for\ \lambda < w_f \\ Y_f(\lambda - w_f) & for\ \lambda \geq w_f \end{cases} \tag{11}$$

where Y_f is the fibril modulus, λ is the fiber stretch ratio defined as the current length normalized by the unloaded length. Each fibril remains unloaded until it becomes taut, indicating that λ is equal to the fibril's waviness, w_f, and hence $\lambda - w_f$ is the linear strain on the fibril. The fiber's engineering stress, σ_e, due to the stress σ_f developed by fibrils with waviness between w_f and $w_f + dw_f$ can be computed as:

$$d\sigma_e = Np(w_f)\sigma_f dw_f, \tag{12}$$

Group	Experimental condition
C ($n=6$)	Stretched intermittently to 10% strain at every 10 min without enzyme
D ($n=13$)	Digested without mechanical interference
D-3 ($n=11$)	Digested in the presence of a static stress (300 kPa)
D-6 ($n=11$)	Digested in the presence of a static stress (600 kPa)
D-i ($n=6$)	Digested while intermittently stretched to 10% strain at every 10 min

Table 1. Digestion conditions using bacterial collagenase.

where N is the total number of fibrils. Replacing $p(w_f)$ and σ_f with Eqs. (10) and (11), respectively, and integrating Eq. (12) across the entire range of waviness provides the relationship between σ_e and λ as follows:

$$\sigma_e = \begin{cases} \frac{Y_f}{B(\alpha,\beta)\alpha(\alpha+1)}(\lambda-1)\left(\frac{\lambda-1}{w_{max}-1}\right)^{\alpha}\left((\alpha+1)A_1-\alpha B_1\right) & for\ 1 \le \lambda < w_{max} \\ \frac{Y_f}{B(\alpha,\beta)\alpha(\alpha+1)}(\lambda-1)\left((\alpha+1)A_2-\alpha B_2\right) & for\ \lambda \ge w_{max} \end{cases} \tag{13}$$

where A_1, B_1, A_2, and B_2 are defined as:

$$\begin{aligned} A_1 &= F_1\left(\alpha; 1-\beta, 1; \alpha+1; \frac{\lambda-1}{w_{max}-1}, 1-\lambda\right), \\ B_1 &= F_1\left(\alpha+1; 1-\beta, 1; \alpha+2; \frac{\lambda-1}{w_{max}-1}, 1-\lambda\right), \\ A_2 &= F_1\left(\alpha; 1-\beta, 1; \alpha+1; 1, 1-w_{max}\right), \\ B_2 &= F_1\left(\alpha+1; 1-\beta, 1; \alpha+2; 1, 1-w_{max}\right). \end{aligned}$$

and F_1 is the Appell hypergeometric function of two variables, defined as

$$F_1\left(a; b, b'; c; x, y\right) = \sum_{m=0}^{\infty}\sum_{n=0}^{\infty}\frac{a_{m+n}b_m b'_n}{m!n!c_{m+n}}x^m y^n,$$

where $(q)_n$ denotes the falling factorial of q. The series in F_1 converges when $|x|<1$ and $|y|<1$. The fiber modulus Y in the linear region of the stress-strain curve (i.e., $\lambda \ge w_{max}$) is obtained by differentiating the Eq. (13) with respect to fiber strain $\epsilon = \lambda - 1$ as $\frac{d\sigma_e}{d\epsilon} = \frac{d\sigma_e}{d\lambda}$, which yields the following relationship:

$$Y = \frac{Y_f}{B(\alpha,\beta)\alpha(\alpha+1)}\left((\alpha+1)A_2-\alpha B_2\right). \tag{14}$$

Experimental fiber stress-strain curves were fitted with Eq. (13) to obtain estimated fibril modulus Y_f using Matlab (MathWorks, MA, USA). Fiber modulus Y was then predicted using Eq. (14).

Computational modeling

To interpret the digestion results, a discrete fiber model was also developed, which consists of a set of parallel and non-interacting fibrils with the mechanical behavior described in Eq. (11). Probabilistic rules were introduced to describe fibril rupture and enzymatic weakening. Accordingly, a fibril was assumed to rupture with probability P_r based on the force F_f it carried at a given stretch ratio and its relative modulus $\frac{Y_{f,n}}{Y_{f,0}}$:

$$P_r = 1 - \frac{Y_{f,n}}{Y_{f,0}} + e^{\frac{F_f}{qF_{f,10}}} - 1 \tag{15}$$

where $q = 4$ was chosen based on preliminary simulations to match experimental observations in the D-i group. Equation (15) includes two parts. The first part, $1 - \frac{Y_{f,n}}{Y_{f,0}}$, increases as the relative fibril modulus decreases with iteration time n due to digestion. For undigested fibrils, $\frac{Y_{f,n}}{Y_{f,0}} = 1$, and hence, this part of P_r vanishes. The second part relates to the force on a fibril with an expression obtained from avalanches in fracture process[50]. When the force on the fibril is zero, $F_f = 0$ and the second part $e^{\frac{F_f}{qF_{f,10}}} - 1 = 0$. Here, the force $F_{f,10}$ is the average fibril force at 10% fiber strain. Between each stretch, F_f=0 for all fibrils while digestion can gradually reduce the modulus and increase P_r. After a fibril failed, its force was set to zero.

The digestion of collagen fibers was simulated such that the effects of the enzyme were applied to the fiber every minute using a probabilistic approach. An exponential relationship between fibril force and digestion probability was motivated by Bell's theory[51] which we previously also used to describe enzymatic digestion of elastic fibers[37]. For each fibril, the following digestion probability was applied:

$$P_d = \frac{C}{w_f}e^{sF_f} \tag{16}$$

where C=0.02 and s =10^{-9} were chosen based on simulation results to match experimental observations in the D group. The modulus of a fibril at timepoint n was $Y_{f,n} = 0.998\,Y_{f,n-1}$ with probability P_d after one iteration and $n = 0, \ldots, 60$. The fiber stress at time n was then computed by summing the forces on the fibrils that have not ruptured. Based on experimental results and applying the analytic model to estimate fibril modulus, a value of 100 MPa was used for $Y_{f,0}$ for all computational simulations. The fibril waviness distribution was simulated based on fitting Eq. (10) to the waviness distribution obtained from SEM imaging. The different digestion protocols were then simulated by changing input parameters including time interval between each stretch, the number of stretches following initial stretch, and the applied force.

Statistical analysis

To compare the waviness distributions of the digested and undigested groups, the Kolmogorov-Smirnov (KS) test was used. The comparison of fiber modulus between different digestion groups was carried out using a one-way ANOVA. A difference was considered statistically significant when $P < 0.05$.

Data availability

The datasets generated and analyzed in the current study are available from the corresponding author on reasonable request.

Received: 21 December 2023; Accepted: 24 October 2024
Published online: 22 November 2024

References

1. Suki, B. *Structure and Function of the Extracellular Matrix: A Multiscale Quantitative Approach* (Academic, 2021).
2. Sicard, D. et al. Aging and anatomical variations in lung tissue stiffness. *Am. J. Physiology-Lung Cell. Mol. Physiol.* **314**, L946–L955. https://doi.org/10.1152/ajplung.00415.2017 (2018).
3. Alves, C. et al. Homeostatic maintenance via degradation and repair of elastic fibers under tension. *Sci. Rep.* **6**, 27474. https://doi.org/10.1038/srep27474 (2016).
4. D'Armiento, J., Dalal, S. S., Okada, Y., Berg, R. A. & Chada, K. Collagenase expression in the lungs of transgenic mice causes pulmonary emphysema. *Cell*. **71**, 955–961. https://doi.org/10.1016/0092-8674(92)90391-o (1992).
5. Yi, E. et al. Mechanical forces accelerate collagen digestion by bacterial collagenase in lung tissue strips. *Front. Physiol.* **7** https://doi.org/10.3389/fphys.2016.00287 (2016).
6. Suki, B., Lutchen, K. R. & Ingenito, E. P. On the progressive nature of emphysema. *Am. J. Respir. Crit Care Med.* **168**, 516–521. https://doi.org/10.1164/rccm.200208-908PP (2003).
7. Fratzl, P. et al. Fibrillar structure and mechanical properties of collagen. *J. Struct. Biol.* **122**, 119–122. https://doi.org/10.1006/jsbi.1998.3966 (1998).
8. Saini, K., Cho, S., Dooling, L. J. & Discher, D. E. Tension in fibrils suppresses their enzymatic degradation: A molecular mechanism for 'use it or lose it'. *Matrix Biol.* **85–86**, 34–46. https://doi.org/10.1016/j.matbio.2019.06.001 (2020).
9. Jawde, S. B. et al. Inflation instability in the lung: An analytical model of a thick-walled alveolus with wavy fibres under large deformations. *J. R. Soc. Interface*. **18**, 20210594. https://doi.org/10.1098/rsif.2021.0594 (2021).
10. Cavalcante, F. S. A. et al. Mechanical interactions between collagen and proteoglycans: Implications for the stability of lung tissue. *J. Appl. Physiol.* **98**, 672–679. https://doi.org/10.1152/japplphysiol.00619.2004 (2005).
11. Franchi, M. et al. Crimp morphology in relaxed and stretched rat Achilles tendon. *J. Anat.* **210**, 1–7. https://doi.org/10.1111/j.1469-7580.2006.00666.x (2007).
12. Svensson, R. B., Mulder, H., Kovanen, V. & Magnusson, S. P. Fracture mechanics of collagen fibrils: Influence of natural cross-links. *Biophys. J.* **104**, 2476–2484. https://doi.org/10.1016/j.bpj.2013.04.033 (2013).
13. Hansen, P. et al. Lower strength of the human posterior patellar tendon seems unrelated to mature collagen cross-linking and fibril morphology. *J. Appl. Physiol.* **108**, 47–52. https://doi.org/10.1152/japplphysiol.00944.2009 (2010).
14. Bailey, A. J., Paul, R. G. & Knott, L. Mechanisms of maturation and ageing of collagen. *Mech. Ageing Dev.* **106**, 1–56. https://doi.org/10.1016/S0047-6374(98)00119-5 (1998).
15. Zhang, G. et al. Development of tendon structure and function: Regulation of collagen fibrillogenesis. *J. Musculoskelet. Neuronal Interact.* **5**, 5–21 (2005).
16. Buckley, M. R. et al. Distributions of types I, II and III collagen by region in the human supraspinatus tendon. *Connect. Tissue Res.* **54**, 374–379. https://doi.org/10.3109/03008207.2013.847096 (2013).
17. Proestaki, M., Burkel, B. M., Galles, E. E., Ponik, S. M. & Notbohm, J. Effect of matrix heterogeneity on cell mechanosensing. *Soft Matter*. **17**, 10263–10273. https://doi.org/10.1039/d1sm00312g (2021).
18. Riley, G. P. et al. Tendon degeneration and chronic shoulder pain: Changes in the collagen composition of the human rotator cuff tendons in rotator cuff tendinitis. *Ann. Rheum. Dis.* **53**, 359–366. https://doi.org/10.1136/ard.53.6.359 (1994).
19. Seyer, J. M., Hutcheson, E. T. & Kang, A. H. Collagen polymorphism in idiopathic chronic pulmonary fibrosis. *J. Clin. Invest.* **57**, 1498–1507. https://doi.org/10.1172/jci108420 (1976).
20. Yang, L. et al. Mechanical properties of native and cross-linked type I collagen fibrils. *Biophys. J.* **94**, 2204–2211. https://doi.org/10.1529/biophysj.107.111013 (2008).
21. Jones, M. G. et al. Nanoscale dysregulation of collagen structure-function disrupts mechano-homeostasis and mediates pulmonary fibrosis. *eLife*. **7**, e36354. https://doi.org/10.7554/eLife.36354 (2018).
22. Andriotis, O. G. et al. Nanomechanical assessment of human and murine collagen fibrils via atomic force microscopy cantilever-based nanoindentation. *J. Mech. Behav. Biomed. Mater.* **39**, 9–26. https://doi.org/10.1016/j.jmbbm.2014.06.015 (2014).
23. Gsell, K. Y., Veres, S. P. & Kreplak, L. Single collagen fibrils isolated from high stress and low stress tendons show differing susceptibility to enzymatic degradation by the interstitial collagenase matrix metalloproteinase-1 (MMP-1). *Matrix Biol. Plus*. **18**, 100129. https://doi.org/10.1016/j.mbplus.2023.100129 (2023).
24. Topol, H., Demirkoparan, H. & Pence, T. J. Fibrillar Collagen: a review of the mechanical modeling of strain-mediated enzymatic turnover. *Appl. Mech. Rev.* **73** https://doi.org/10.1115/1.4052752 (2021).
25. Chang, S. W., Flynn, B. P., Ruberti, J. W. & Buehler, M. J. Molecular mechanism of force induced stabilization of collagen against enzymatic breakdown. *Biomaterials*. **33**, 3852–3859. https://doi.org/10.1016/j.biomaterials.2012.02.001 (2012).
26. Flynn, B. P. et al. Mechanical strain stabilizes reconstituted collagen fibrils against enzymatic degradation by mammalian collagenase matrix metalloproteinase 8 (MMP-8). *PLOS ONE*. **5**, e12337. https://doi.org/10.1371/journal.pone.0012337 (2010).
27. Saini, K. et al. Heterogeneous strains in tissue collagen show that high strains locally suppress degradation by collagenase. *bioRxiv* (2021). https://doi.org/10.1101/2021.02.07.430141
28. Zareian, R. et al. Probing collagen/enzyme mechanochemistry in native tissue with dynamic, enzyme-induced creep. *Langmuir*. **26**, 9917–9926. https://doi.org/10.1021/la100384e (2010).
29. Camp, R. J. et al. Molecular Mechanochemistry: Low force switch slows enzymatic cleavage of human type I collagen Monomer. *J. Am. Chem. Soc.* **133**, 4073–4078. https://doi.org/10.1021/ja110098b (2011).
30. Adhikari, A. S., Chai, J. & Dunn, A. R. Mechanical load induces a 100-Fold increase in the rate of Collagen Proteolysis by MMP-1. *J. Am. Chem. Soc.* **133**, 1686–1689. https://doi.org/10.1021/ja109972p (2011).
31. Adhikari, A. S., Glassey, E. & Dunn, A. R. Conformational dynamics accompanying the proteolytic degradation of trimeric collagen I by collagenases. *J. Am. Chem. Soc.* **134**, 13259–13265. https://doi.org/10.1021/ja212170b (2012).
32. Yeganegi, A., Whitehead, K., de Castro Brás, L. E. & Richardson, W. J. Mechanical strain modulates extracellular matrix degradation and byproducts in an isoform-specific manner. *Biochim. et Biophys. Acta (BBA) - Gen. Subj.* **1867**, 130286. https://doi.org/10.1016/j.bbagen.2022.130286 (2023).

33. Huang, C. & Yannas, I. V. Mechanochemical studies of enzymatic degradation of insoluble collagen fibers. *J. Biomed. Mater. Res.* **11**, 137–154. https://doi.org/10.1002/jbm.820110113 (1977).
34. Ruberti, J. W. & Hallab, N. J. Strain-controlled enzymatic cleavage of collagen in loaded matrix. *Biochem. Biophys. Res. Commun.* **336**, 483–489. https://doi.org/10.1016/j.bbrc.2005.08.128 (2005).
35. Vargaftig, B. B., Lefort, J. & Giroux, E. L. Haemorrhagic and inflammatory properties of collagenase fromC. Histolyticum. *Agents Actions.* **6**, 627–635. https://doi.org/10.1007/BF01971582 (1976).
36. Janwitthayanan, W. et al. In vivo gene expression and immunoreactivity of Leptospira collagenase. *Microbiol. Res.* **168**, 268–272. https://doi.org/10.1016/j.micres.2012.12.005 (2013).
37. Araújo, A. D. et al. Dynamics of enzymatic digestion of elastic fibers and networks under tension. *Proc. Natl. Acad. Sci. USA.* **108**, 9414–9419. https://doi.org/10.1073/pnas.1019188108 (2011).
38. Jesudason, R. et al. Mechanical forces regulate elastase activity and binding site availability in lung elastin. *Biophys. J.* **99**, 3076–3083. https://doi.org/10.1016/j.bpj.2010.09.018 (2010).
39. Perumal, S., Antipova, O. & Orgel, J. P. R. O. Collagen fibril architecture, domain organization, and triple-helical conformation govern its proteolysis. *Proc. Natl. Acad. Sci.* **105**, 2824–2829 (2008). https://doi.org/10.1073/pnas.0710588105
40. Zhu, J., Hoop, C. L., Case, D. A. & Baum, J. Cryptic binding sites become accessible through surface reconstruction of the type I collagen fibril. *Sci. Rep.* **8**, 16646. https://doi.org/10.1038/s41598-018-34616-z (2018).
41. Liao, H. & Belkoff, S. M. A failure model for ligaments. *J. Biomech.* **32**, 183–188. https://doi.org/10.1016/S0021-9290(98)00169-9 (1999).
42. Watanabe-Nakayama, T., Itami, M., Kodera, N., Ando, T. & Konno, H. High-speed atomic force microscopy reveals strongly polarized movement of clostridial collagenase along collagen fibrils. *Sci. Rep.* **6**, 28975. https://doi.org/10.1038/srep28975 (2016).
43. Mirzarafie, A. et al. A fast and mild decellularization protocol for obtaining extracellular matrix. *Rejuvenation Res.* **17**, 159–160. https://doi.org/10.1089/rej.2013.1488 (2014).
44. Hoffmann, G. A. & Smith, M. L. New insights into Collagen and fibronectin reciprocity during extracellular matrix formation. *Chem*. **5**, 1930–1932. https://doi.org/10.1016/j.chempr.2019.07.012 (2019).
45. Klotzsch, E. et al. Fibronectin forms the most extensible biological fibers displaying switchable force-exposed cryptic binding sites. *Proc. Natl. Acad. Sci.* **106**, 18267–18272. https://doi.org/10.1073/pnas.0907518106 (2009).
46. Malaspina, D. C., Szleifer, I. & Dhaher, Y. Mechanical properties of a collagen fibril under simulated degradation. *J. Mech. Behav. Biomed. Mater.* **75**, 549–557. https://doi.org/10.1016/j.jmbbm.2017.08.020 (2017).
47. Eckhard, U., Schönauer, E., Nüss, D. & Brandstetter, H. Structure of collagenase G reveals a chew-and-digest mechanism of bacterial collagenolysis. *Nat. Struct. Mol. Biol.* **18**, 1109–1114. https://doi.org/10.1038/nsmb.2127 (2011).
48. Bradshaw, M. J., Hoffmann, G. A., Wong, J. Y. & Smith, M. L. Fibronectin fiber creep under constant force loading. *Acta Biomater.* **88**, 78–85. https://doi.org/10.1016/j.actbio.2019.02.022 (2019).
49. Frisch, K. E. et al. Quantification of collagen organization using fractal dimensions and Fourier transforms. *Acta Histochem.* **114**, 140–144. https://doi.org/10.1016/j.acthis.2011.03.010 (2012).
50. Zapperi, S., Ray, P., Stanley, H. E. & Vespignani, A. Avalanches in breakdown and fracture processes. *Phys. Rev. E.* **59**, 5049–5057. https://doi.org/10.1103/PhysRevE.59.5049 (1999).
51. Bell, G. I. models for the specific adhesion of cells to cells. *Science.* **200**, 618–627. https://doi.org/10.1126/science.347575 (1978).

Acknowledgements

Research reported in this publication was supported by the Boston University Micro and Nano Imaging Facility and Precision Measurement Laboratory.

Author contributions

YD, EBS and BS conceived the research; YD and YW carried out experiments; EBS, JH and YD isolated collagen fibers; MN and JHK analyzed images; JH, JHK, MLS and KRL contributed to various aspects of design and interpretation; YD, JH and BS wrote manuscript.

Funding

The authors acknowledge support from the National Institutes of Health award U01 HL139466 and the Center for Multiscale & Translational Mechanobiology.

Declarations

Competing interests

The authors declare no competing interests.

Additional information

Supplementary Information The online version contains supplementary material available at https://doi.org/10.1038/s41598-024-77704-z.

Correspondence and requests for materials should be addressed to B.S.

Reprints and permissions information is available at www.nature.com/reprints.

Publisher's note Springer Nature remains neutral with regard to jurisdictional claims in published maps and institutional affiliations.